A Reproduction of Condensed Phase Phenomena with the TIP4P/2005 Model of Water

Ian Harreschou[1], Harry Winston Sullivan[1]

[1] Department of Chemical Engineering and Material Science, Amundson Hall, 421 Washington Ave SE #151 Minneapolis, MN 55455

Abstract :

In this work, we re-create the findings reported by Abascal and Vega, who present a novel, general purpose rigid four site water model (Abascal et al., 2005 "A general purpose model for the condensed phases of water: TIP4P/2005". In: The Journal of Chemical Physics 123.23, p. 234505. issn: 0021-9606. doi: 10.1063/1.2121687.). This parameterization offers generality and applicability in calculating many target properties across a wide swath of input conditions, as well as greater computational efficiency. Herein, we utilize the TIP4P/2005 model to calculate various quantities of interest; density ($\rho(T)$, $\rho(P)$), expansivity (α_P), isothermal compressibility (κ_T), liquid-phase pair distribution function ($g_{OO}(r)$), self-diffusion coefficient (D), the L-*Ih* polymorph phase equilibrium line, the heat capacity C_p, and a high pressure equation of state.

Production simulations are performed using LAMMPS. An oxygen-oxygen Lennard-Jones interaction with long-range corrections and a particle-particle particle-mesh (*pppm*) solver for Coulombic interactions are applied for the interatomic potential. Molecules are made rigid via the SHAKE method before being placed in the *NPT* ensemble. Thermodynamic integration and the calculation of quantities of interest (QOIs) were performed in Python *post-hoc*.

1 Article Review

1.1 Summary

Molecular models are often optimized with respect to specific quantities of interest (QOIs) to ensure accurate behavior for a target application. The choice of these QOIs varies from study to study, depending on specific needs. For the study of water in particular, this issue is exacerbated by the diverse range of systems in which it plays a vital role. These span from fundamental studies of quantum behavior, standard physical chemistry applications, and as a solvent for biological systems. Further complicating matters, the assumptions underlying water models vary substantially. Specifically, parameters such as molecular rigidity, charge distribution or magnitude, and degree of truncation in many-body energy expansions are selected inconsistently from paper to paper.

As a result, there exists a zoo of distinct water models, each well-suited for different purposes. Therefore, it is of utmost importance to identify a general-purpose model with well-founded assumptions and broad applicability across the phase diagram for routine use. The authors, J. L. F. Abascal and C. Vega, aimed to do exactly this. Their TIP4P/2005 model of water proposes a four-site rigid molecule containing three partial charges and one Lennard-Jones site. A massless dummy atom was introduced to better capture the charge distribution of real water, and to promote more realistic emergent properties. This site displaces the partial charge from the oxygen atom toward the hydrogen atoms, positioning it along the HOH bisector at a distance r_{OM}. A schematic of the molecular geometry is provided in Figure 1.

The functional form of the interatomic potential for this model has two contributions; a modified Lennard-Jones term, as well as electrostatic interactions between pairs.

$$U_{\text{LJ}} = 4\epsilon\left[\left(\frac{\sigma}{r_{\text{OO}}}\right)^{12} - \left(\frac{\sigma}{r_{\text{OO}}}\right)^{6}\right], \tag{1}$$

$$U_{\text{electrostatic}} = \frac{1}{4\pi\epsilon_0}\sum_{a,b}\frac{q_a q_b}{r_{ab}}. \tag{2}$$

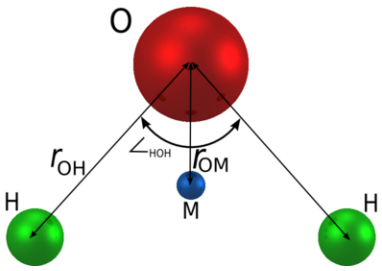

Figure 1. The TIP4P rigid water molecule with a faux massless charged atom along the HOH bisector. Taken from `http://www.sklogwiki.org/SklogWiki/index.php/TIP4P_model_of_water`.

The parameters σ and ϵ represent the effective particle diameter and the depth of the Lennard-Jones potential between oxygen atoms, respectively, at a separation distance r_{OO}. The electrostatic interaction is governed by the charges q_a and q_b, and their separation distance r_{ab}. Due to the overall neutrality of the water molecule, it follows that $q_H = -\frac{1}{2}q_M$, making the charges linearly dependent.[1]. In summary, the TIP4P model is characterized by the geometry shown in Figure 1, along with four tunable parameters denoted by $\xi = \{\sigma, \epsilon, q_H, r_{OM}\}$.

The authors argue that the work by Paschek, 2004 implies density effects must be considered as a QOI if the potential is intended for studies of hydrophobicity. Specifically, the existence of a low-pressure isobaric density maximum as a function of temperature, denoted T_{md}, needs to be reproduced. Furthermore, the authors aim to have a "reasonable" description of the solid phases; while the TIP4P geometry reproduces qualitative behavior, the SPC/E and TIP5P models do not. Their inability can be traced back to the interatomic potentials induced excessive stability of ice *II*. Each polymorph consists of a different hydrogen bonding network, im-

[1] The subscript M on the charge emphasizes that the oxygen site carries no charge and it is specifically on the massless dummy atom.

plying the need for the interatomic potential to be applicable for a variety of crystal structures, as well as in the liquid phase.

1.1.1 The Fitting Procedure In order to fit the parameters of their model they utilize m QOIs $\psi_j(\xi)$ and minimize the weighted sum of squares

$$\mathcal{L}(\xi) = \sum_{j=1}^{m} w_j \left(\psi_j(\xi) - \psi_j^{\text{expt}}\right)^2 \tag{3}$$

where ξ is the set of n model parameters $\xi = \{\xi_1, \dots \xi_n\}$ and ψ_j^{expt} is the experimental observation of the jth QOI. The authors then perform a sequential optimization. Based off the information given, we believe they used a gradient based procedure of the form

$$\xi_i^{(k+1)} = \xi_i^{(k)} - \frac{\partial \mathcal{L}(\xi^{(k)})}{\partial \xi_i} \tag{4}$$

$$= \xi_i^{(k)} - 2w_i \left(\psi_j(\xi^{(k)}) - \psi_j^{\text{expt}}\right) \frac{\partial \psi_i(\xi^{(k)})}{\partial \xi_i}. \tag{5}$$

Rather than use analytical differentiation of the cost function, the authors opted for numerical differentiation through a forward difference of the form

$$\frac{\partial \psi_i}{\partial \xi_i}(\xi^{(k)}) \approx \frac{\psi_i(\xi^{(k)}) - \psi_i(\xi^{\text{ref}})}{\xi_i^{(k)} - \xi_i^{\text{ref}}} \tag{6}$$

where ξ^{ref} is a reference set of parameters which differ only in the ith model parameter. Within the paper they do not explicitly state the reference, therefore we assumed it changes throughout optimization to ensure local accuracy of the gradient.

Their choices of ψ will heavily affect the predictiveness of their model, in that their choices determine where the model is considered *good*, i.e. within the convex hull of the training domain, and where it is bad, outside of this hull.[2] The authors argue that the temperature of maximum density T_{md} should be fit at the cost of a degradation in the predicted melting temperature T_m.

The experimental difference between T_m and T_{md} is only about 4 K at 1 bar, however for TIP4P-like molecules, there is an empirically observed difference of 22 K (Vega et al., 2005). Therefore, one must be sacrificed at the expense of the other. Furthermore, the authors argue that the relation between T_m and T_{md} may not be as clear as it seems. The introduction of polarization effects and deuteration through quantum calculation can change the difference to 7 K. A majority of the deviation is due to a shift in T_m, which is more acutely affected by the hydrogen bonding structure.

The key insight is that fitting both simultaneously may be a fool's errand. It is not fully understood what assumptions are required to produce this emergent behavior, and it is known that it can't be done with a 4 site model. These insights are used to motivate T_{md} as a particular instance of ψ_i as opposed to T_m. A similar argument can be made for the enthalpy of vaporization.

At the time of publication, the use of $g(r)$ as a fitting target seemed dubious at best. Only recently had experimental determinations of $g(r)$ through neutron and X-ray scattering converged to a similar answer. This gave the authors skepticism due to its recency. Hence, they do not treat $g(r)$ as a direct optimization target, though it does not imply that $g(r)$ should not be qualitatively similar. They also selected the densities of ices *II* and *V* as targets.

This gives the set of optimization targets ψ as: T_{md}, the enthalpy of vaporization, liquid density at ambient conditions, the densities of ice *II* and *V* at 123 K and 0 MPa, and 223 K and 530 MPa, respectively, as well as the density of ice *III* at 300 MPa for a variety of temperatures where it remains stable.

Fitting these properties efficiently requires a method of inferring points along phase coexistence quickly. Typically their discovery requires the need for advanced sampling in order to induce nucleation of one phase from another, or other expensive techniques based off interfaces. This difficulty may be avoided entirely with a clever use of thermodynamic integration.

1.1.2 Prediction of Phase Behavior Under a Change in Potential with Thermodynamic Integration For an arbitrary model, inferring phase coexistence lines can be exceedingly difficult. However, if coexistence is known for a reference model, extrapolation becomes feasible via integration of a generalized Clapeyron equation. By expressing the Gibbs free energy in terms of its natural variables T and P, one can introduce variation in the interatomic potential parameters as an additional generalized variable λ. Specifically, Abascal and Vega used λ as an interpolation parameter between a reference potential and a target potential.

$$U(\lambda) = (1-\lambda)U_{\text{ref}} + \lambda U_{\text{new}} \tag{7}$$

If $\lambda = 1 \implies U = U_{\text{new}}$, if $\lambda = 0 \implies U = U_{\text{ref}}$. This would give an expansion of $G(T, P, \lambda)$ into partials as

$$dG = -SdT + VdP + X_g d\lambda \tag{8}$$

where

$$X_g = \left(\frac{\partial G}{\partial \lambda}\right)_{NPT}. \tag{9}$$

One can show through an equilibrium fluctuation theorem that this is equivalent to the expectation (Frenkel et al., 2002).

$$X_g = \left\langle \frac{\partial U}{\partial \lambda} \right\rangle_{NPT\lambda}. \tag{10}$$

Using these relations, the authors are able extrapolate (T, P) equilibrium points of U_{ref} to predict the state point parametrized by U_{new}. Specifically they use the following.

$$\frac{dT}{d\lambda} = \frac{\Delta X_g}{\Delta S}, \quad \frac{dP}{d\lambda} = -\frac{\Delta X_g}{\Delta V}. \tag{11}$$

This scheme provides a differential equation for the curve $P(\lambda)$ and $T(\lambda)$ along the line of phase equilibrium $dG_S = dG_L$.

1.1.3 Presented Results The authors took their optimization procedure and determined an optimal fit of the parameters to be:

$$\epsilon/k = 93.2\ [K], \quad \sigma = 3.1589\ [\text{Å}] \tag{12}$$

$$q_H = 0.5564\ [e], \quad r_{OM} = 0.1546\ [\text{Å}] \tag{13}$$

The authors also present the dipole moment and quadrupole moment components as the change in r_{OM} causes deviation from previous modeling assumptions. The moments were 6% higher than

[2] While there is a technical definition of the hull, we mean this in more colloquial sense.

previous 4 site models (TIP4P, TIP4P/Ew). Afterwards, a smorgasbord of emergent properties are shown, calculating with Monte Carlo NPT simulation and NVE dynamics. Rather than go into detail about how these properties are calculated from a molecular simulation, we present key findings and save the details for Section 3.

For most properties ($\rho, \kappa_T, C_p, \Delta_v H, \epsilon, D$) at ambient conditions, the TIP4P/2005 model performed remarkably well despite the lack of inclusion as directly optimized QOIs. The same trend of highly accurate fitting persisted in the density ρ as a function of temperature T. Their results predict $T_{md} = 278\ K$ at $\rho = 1.0005\ g/cm^3$ for a pressure of 1 bar. As we will see later this is in excellent agreement with experiment. These results are then propagated through a chain rule to predict the thermal expansion coefficient.

$$\alpha_P = -\frac{1}{V}\left(\frac{\partial V}{\partial T}\right)_P = \left(\frac{\partial \ln \rho}{\partial T}\right)_P \tag{14}$$

By applying a 5th order power series fit with respect to inverse temperature $1/T$ to $\rho(T) = a + b/T + c/T^2 \ldots f/T^5$, the analytical derivative may be taken to determine α_P within an interpolated range. Again the TIP4P/2005 model gives excellent agreement.

A similar strategy of running simulations at a fixed condition, applying a polynomial fit to a quantity, and taking the derivative was done for the isothermal compressibility κ_T and the constant pressure heat capacity C_p. The compressibility matched experiment much closer than the heat capacity, although C_p was still quite close.

The model was also used to study different ice polymorphs and their associated densities. TIP4P/2005 was able to obtain a high quality of fit, however there is a clear deviation from experiment which can be overcome by TIP4P/Ice. The authors also compare every TIP4P like models density and demonstrate a clear trend with the type of polymorph. If you order models by the size of their error (accounting for both positive and negative deviations), their resulting bar charts are all roughly the in same order (*II*, *IV*, *XI*, *Ic*, *VI*, *XII*, *Ih*, *IX*, *V*, and *III*). TIP4P/2005 also provides a high quality of fit in the liquid state at high pressures and temperatures as seen by the equation of state. This demonstrates the ability for the model to be used outside of ambient conditions.

The authors also showed the phase diagram as a function of (T, P). They computed this via the integration scheme outlined above when they changed from one potential to another as well as typical Clapeyron thermodynamic integration. A fourth-order Runge-Kutta algorithm was used implying there was four simulations per state point, and potentially 8 if they utilized multiple boxes for their simulation. Their results were lack luster in comparison to TIP4P/Ice, however still had qualitative improvements in comparison to most water models. The remaining observables they computed were the radial distribution function, the dielectric constant as well as the enthalpy of vaporization with a self-polarization correction term. All of which showed quantitative agreement with experiment and provided a strong improvement in comparison with classic TIP4P.

Their results demonstrated TIP4P/2005's capability of handling temperature ranges from 123 to 573 K and pressures up to 40,000 bar. Their model is a distinct improvement to the previous generalist model TIP4P/Ew in every property except the enthalpy of vaporization and dielectric constant, which were only marginally worse in TIP4P/2005. The broad range of applicability of this model poses it as the workhorse water model for biomolecular simulation. The authors believe that within the confines of classical simulation that TIP4P/2005 is as reliable as you can get given the assumptions.

1.2 Critical Assessment

The work by Abscal and Vega represents the pinnacle of water force field developments. As of May 2025 it has garnered over 4,000 citations, and this is no accident. The paper and proposed model is both sensible in terms of computational cost and provides reasonable predictions. The simulation community clearly prefers this semi-empirical strategy given the 6,120 hits on google scholar when looking up "tip4p2005 water". For all its strengths there are certainly drawbacks of the model as well as the pedagogy within the paper itself. Namely the description of the optimization process and the details on the simulations seemed to lack sufficient details for exact reproduction.

Before examining the flaws and places where it may be improved, we first acknowledge all the things it did right. Firstly, the choice of optimization target is well justified with numerous publications backing up their reasoning. The art of dataset choice and QOI targets is becoming clouded in the modern corpus of force field optimization due to the rise of larger neural network models or purely data-driven methods. Around 2005, there certainly was significant development of complex force field methods given the the popularity of Gaussian processes (Rasmussen et al., 2008), which were at the forefront of potential energy surface approximation Gibbs, 1998. TIP4P/2005 is no different and we believe that this is why their model performs so well across the phase diagram despite simple.

Another feature of their work is the sheer amount of observables computed for their model, as well as TIP4P/Ice, TIP4P/Ew, and TIP5P models. This allows the reader to get a more wholistic view of where TIP4P/2005 stands for their target application. This is effectively a large cross validation set, which helps certify the generalist nature of their model. If they had not done this comparison, their model surely would not have gotten as much attention as it did. Not only this but they provided reference models to account for the typical pitfalls of the TIP4P/2005 model, giving the authors major credibility.

The last thing this model did well was consider the application at the first step of the optimization process. Surely any decent computational chemist could create a water model to fit most properties shown here if they had enough compute. With the proliferation of DFT functionals, higher level theory, and Moore's law speeding up computation this is bound to happen eventually. However this strategy lacks the practicality present in Abascal and Vega's work. By enforcing rigid bonds and minimal non-bonded interaction terms, they were able to make an immensely efficient model, lending it to become the prime candidate for biological systems where simulation of millions of atoms are needed.

Despite all the things they did right there was certainly a lack of pedagogy in the paper. Whether or not this is the place to be pedagogical is another question. In our personal view, teaching the reader is one of the best things a paper can do for the purpose of reproducible science. Most of the results sections give sufficient detail in the post processing required to compute the plots, however the simulations themselves are not well described. There is a clear lack in details of the Monte Carlo algorithm.

As an example they mention the use of Ewald summation for the long range portion of the potential and then give a comment about how a screening parameter was "carefully selected for each phase" which is mostly meaningless as there are no details as to how this selection is done. Similarly they do not mention their treatment of rigidness in the Monte Carlo calculation nor do they mention the number of steps used before the Metropolis criteria is applied. There is even a lack of description to how many samples were obtained to compute their observables. Perhaps these details are unneeded for an expert, however for us sorting these out proved to be a major difficulty. Even now we are not entirely certain if our simulations are even comparable to theirs and this might be the reason for the slight deviation in our predictions. The last key thing they did not provide was the Runge-Kutta step size used to trace the phase diagram, which if they had would have saved us a ton of time in our reproduction.

1.3 Suggestions for Improvement

The major places for improvement of the paper is a better description of the simulation methodology and optimization procedure. While the Journal of Chemical Physics may not necessarily be the place for this sort of writing style, it should at least be described well enough for reproduction within the supporting information. Perhaps the simulation details can be swept under the table as the target audience is expected to know these details. However the optimization procedure certainly can't be. Even today optimization is not as well known to computational chemists as it ought to be. A significant expansion of equations fully defining the iteration procedure would add a lot to the paper.

Scientifically speaking, the paper could benefit from a more extensive analysis of the cost surface of the parameters. In fact this sort of analysis has been done on course grained water models (Jacobson et al., 2014). A clear improvement that relies on minimal extra work would be an analysis using the Fisher information metric. They are already acquiring the derivative of the QOI via finite difference, therefore this addition is a trivial extension computationally. Of course a much better extension that could add the same uncertainty quantification as well as more would be a Monte Carlo sampling scheme on the parameters. This would require a major shift in the optimization entirely and may not be well within the scope of the paper as presented.

Being picky, another small place this paper could be improved is consistency in the plotting. Throughout the work the color for the experimental data, the TIP4P/Ew, and the TIP4P/2005 model keep swapping. Similarly the symbols used swap from plot to plot as well. Sometimes TIP4P/2005 is a solid red line and others it is blue star symbols. This led to initial confusion and is honestly not that much to ask for a paper coming out of the Journal of Chemical Physics.

Finally, we look at their Figure 5, which shows the difference of model and experimental densities, $\rho - \rho_{\text{exp}}$. This plot shows a pretty clear trend across each of the water models with respect to polymorphs. It appears the results are all scaled or shifted from one to the next, but they share the same behavior, potentially indicating more systematic differences between the different models. This plot could likely be the topic of another entire research paper, which may disqualify this good critique for a reviewer, but it is only accompanied by a few short sentences. Expanding on its implications would have added much to the paper.

2 Proposed Work

The target article sought to develop an accurate and general model of the potential of water such that it can recreate experimental condensed phased properties while being less computationally intensive. This optimized, rigid molecular water model can be used to calculate thermodynamic properties; phase diagrams for liquid and solid phases, melting and vaporization properties, dielectric constants, pair distribution functions, and self-diffusion coefficients. Each phase diagram is computed via thermodynamic integration, more specifically Hamiltonian Gibbs-Duhem integration.

Ideally we'd be able to reproduce the results and methodology exactly as stated in the paper. However, the authors employed Monte Carlo sampling methods in their constant pressure and temperature simulations in *DLPOLY*. As such, we moved entirely to using molecular dynamics with LAMMPS. The authors compare multiple models for water against experiments to assess their modeling successes, and as such we would like to compare at least two water models; TIP3P and TIP4P, implemented in LAMMPS. If time allows, we would expand on this in the way of including comparisons using a 5 point water model, and by comparing the long-range Lennard-Jones potential used to ML-IAPs available on OpenKIM.

As part of this recreation, we aim to create a series of Python scripts that batch LAMMPS input files at appropriate simulation conditions to the MSI cluster, to run concurrent calculations. SLURM scripts are also utilized where appropriate to loop over input conditions. Data for the majority curves are generated primarily in the NPT ensemble, barring the calculating of self-diffusion which required NPT, NVT, and NVE.

3 Results

3.1 Work Performed and Findings

3.1.1 A Basic Simulation Scheme To study the TIP4P/2005 potential we applied the basic scheme outlined in `https://docs.lammps.org/Howto_tip4p.html`. Most of our simulations were initialized in the liquid state, therefore we opted to pre-equilibrate one at standard temperature and pressure as to spend minimal time later on. For systems in which modeling of solid phases was required, we applied the *genice2* Python package, a so-called "Swiss army knife to generate hydrogen-disordered ice structures" (Matsumoto et al., 2024). This allowed us to quickly generate initial structures in the correct phase, followed by an equilibration run at the appropriate conditions, helping the system potentially reach equilibrium quicker.

On top of the OO Lennard-Jones interaction, the water molecules also interact via Coulomb's law. Due to the potential decaying slower than $r^{1/3}$, a simple tail correction becomes unreliable. The inherent long-ranged nature of the force requires more advanced method than simply truncating the potential. The TIP4P/2005 paper applied an Ewald summation technique, however we opted for the particle-particle partial mesh (PPPM) method due to the size of our system (2000 to 4000 molecules compared to their 360) as well as the $O(N \log N)$ complexity of PPPM. Furthermore, PPPM is easily accelerated by CUDA FFT libraries already implemented in LAMMPS on GPUs.

The standard choice for our thermo-barostat was the Nose-Hoover method with an extended phase space as implemented

in LAMMPS under **fix npt**. The damping parameters for the thermo and barostat were always $T_{damp} = 100 \cdot dt$ and $P_{damp} = 1000 \cdot dt$ as recommended by Axel (see: `https://matsci.org/t/barostat-damp-factor/31483`). Our determination of the equilibration and production periods varied from calculation to calculation, and are discussed as they are presented.

3.1.2 Low- Pressure Isobaric Density Maximum The calculation of the low-pressure isobaric density maximum was computed via sequential simulations at $P = 1$ bar over a range of temperatures T = [250 K, 370 K] in increments of 10 K. This was implemented via a LAMMPS loop alongside post processing to obtain the curve in question. We expect the match to experiment of this curve to be quite high as T_{md} was a directly optimized QOI. In this instance the simulations were run with a timestep of $dt = 1$ fs with a equilibration time of 50,000 fs and production of 200,000 fs.

In order to ensure validity of the results, we applied a time series uncertainty analysis following the methods of Allen et al., 2017. We define the statistical inefficiency s for an observable $\mathcal{A}$ as

$$s = \lim_{\tau_{\text{blk}} \to \infty} s(\tau_{\text{blk}}) \tag{15}$$

where τ_{blk} is the size of a block of the time series and

$$s(\tau_{\text{blk}}) = \frac{\tau_{\text{blk}}\, \sigma^2\left((\mathcal{A})_{\text{blk}}\right)}{\sigma^2(\mathcal{A})} \tag{16}$$

with the block variance computed as

$$\sigma^2\left((\mathcal{A})_{\text{blk}}\right) = \frac{1}{n_{\text{blk}} - 1} \sum_{b=1}^{n_{\text{blk}}} \left(\langle \mathcal{A} \rangle_b - \langle \mathcal{A} \rangle_{\text{run}}\right)^2 \tag{17}$$

and the full-run variance defined by

$$\sigma^2(\mathcal{A}) = \left\langle \delta\mathcal{A}^2 \right\rangle_{\text{run}} = \frac{1}{\tau_{\text{run}} - 1} \sum_{\tau=1}^{\tau_{\text{run}}} \left(\mathcal{A}(\tau) - \langle \mathcal{A} \rangle_{\text{run}}\right)^2 . \tag{18}$$

The block and full-run averages are given by

$$\langle \mathcal{A} \rangle_b = \frac{1}{\tau_{\text{blk}}} \sum_{\tau \in b} \mathcal{A}(\tau) \tag{19}$$

$$\langle \mathcal{A} \rangle_{\text{run}} = \frac{1}{\tau_{\text{run}}} \sum_{\tau=1}^{\tau_{\text{run}}} \mathcal{A}(\tau). \tag{20}$$

The limit of the statistical inefficiency, roughly speaking, is the correlation time of the time series. s is the limiting ratio of the observed variance of an average to the limit as if the time series was generated by an uncorrelated Gaussian process. A plot of $s(\tau)$ is shown in Figure 2.

The limiting s may also be used to compute the deviation from the mean with

$$\sigma^2\left(\langle \mathcal{A} \rangle_{\text{run}}\right) = s\, \frac{\sigma^2(\mathcal{A})}{\tau_{\text{run}}}. \tag{21}$$

We approximated the limiting value as the average between $\tau_{\text{blk}} = 100$ and $\tau_{\text{blk}} = 150$. This choice was made due to the large amount of noise at large times and looking at the plots should most certainly be considered a lower bound especially at lower temperatures. Ideally we would run a longer simulation in order to get better statistics about the limiting value. Notice the interesting

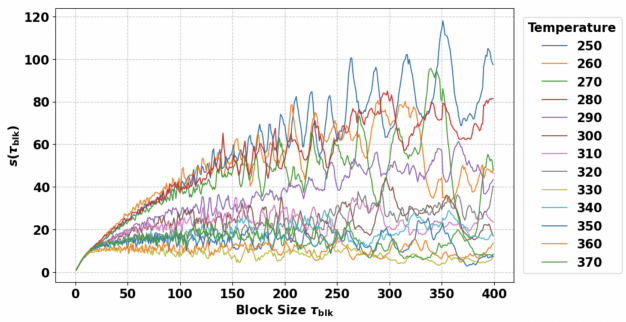

Figure 2. Statistical inefficiency of the density $\mathcal{A} = \rho$ denoted $s(\tau_{\text{blk}})$ as a function of block size τ_{blk} at $P = 1$ bar, shown for a range of temperatures from 250 K to 370K.

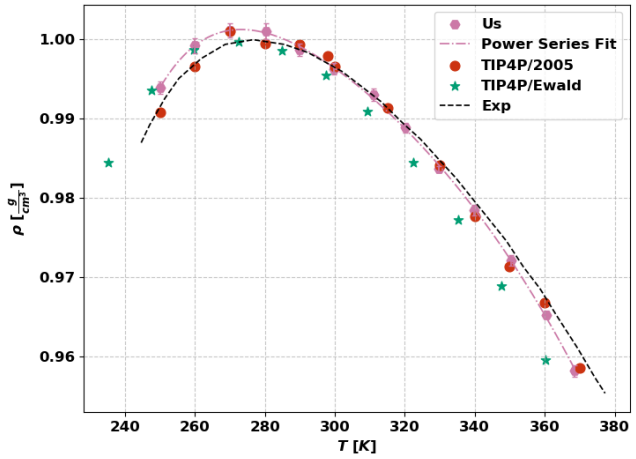

Figure 3. Liquid-phase densities predicted by TIP4P/2005 (authors: red circles, us: pink hexagons), TIP4P/Ewald (authors: green stars), and as measured in experiments. The 5th-order power series fit of $\rho(T)$ for our data is shown in pink. P = 1 bar.

split occurring at 280 K and lower, this may be due to some hysteresis taking place at low temperature. Taking these formulas and applying them to the low-pressure isobaric density as a function of temperature results in the error bars shown in Figure 3.

From these results we then fit a polynomial of the form

$$\rho(T) = a + \frac{b}{T} + \frac{c}{T^2} + \frac{d}{T^3} + \frac{e}{T^4} + \frac{f}{T^5} \tag{22}$$

for unknown constants $a, b, \ldots f$. While we should be applying a Bayesian fit to gauge the uncertainty in the coefficients we simply applied **np.polyfit** because we did not believe the uncertainty was crucial to the analysis at this point. This resulted in coefficients being

$$a = -7.8364 \quad b = 1.1576 \times 10^4 \quad c = -6.1101 \times 10^6 \tag{23}$$

$$d = 1.6113 \times 10^9 \quad e = -2.1033 \times 10^{11} \quad f = 1.0748 \times 10^{13}. \tag{24}$$

3.1.3 Expansivity The expansivity, or thermal expansion coefficient α_P, represents the effective change in size of a material under a change in temperature at constant pressure. Expansivity is

defined by equation 14 as a logarithmic derivative of the density. Applying this to our polynomial gives

$$\alpha_P = -\frac{bT^4 + 2cT^3 + 3dT^2 + 4eT + 5f}{T\left(aT^5 + bT^4 + cT^3 + dT^2 + eT + f\right)}. \tag{25}$$

We can see that this results in a strong fit to both experimental data, as well as the reported results by Abascal and Vega. α_P is also readily computed by a fluctuation formula of the form

$$\left\langle \delta V\, \delta(\mathcal{H} + PV) \right\rangle_{NPT} = k\, T^2\, V\, \alpha_P \tag{26}$$

In this expression, $\delta V = V - \langle V \rangle_{\text{run}}$ and $\delta(\mathcal{H} + PV) = (\mathcal{H} + PV) - \langle \mathcal{H} + PV \rangle_{\text{run}}$ represent the instantaneous deviations of the volume and enthalpy from their respective time-averaged values over the simulation as defined by equation 20. These results show close agreement with the analytical result of equation 25, as seen in figure 4.[3]

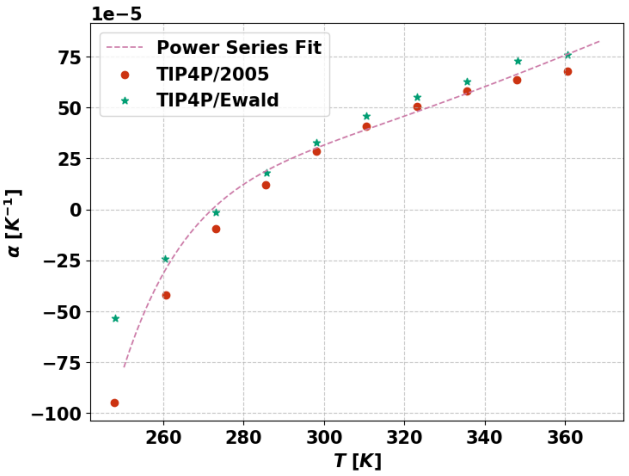

Figure 4. Expansivity of liquid water for P = 1 bar across a range of temperatures. Authors' results are shown with red circles (TIP4P/2005) and green stars (TIP4P/Ewald). Our power series fit (derivative of a 5th order fit of density versus temperature) is shown as a dashed magenta line.

3.1.4 Isothermal Compressibility The isothermal compressibility represents the effective change in volume of a material as you change the pressure at constant temperature. It is given by

$$\kappa_T = -\frac{1}{V}\left(\frac{\partial V}{\partial P}\right)_T. \tag{27}$$

We performed the calculation of this very similarly to the expansion coefficient. By performing sequential simulations at $T = 298$ K, with $P \in [0\text{ bar}, 1000\text{ bar}]$, incrementing by 200 bar. The simulations were run with a timestep of $dt = 1$ fs with a equilibration time of 50000 fs and production of 150000 fs. We then performed a polynomial fit of the form

$$V(P) = g + hP + iP^2 \tag{28}$$

[3] You might notice a clear lack of the fluctuation formula being present in this plot. We suspect something off in the simulations as they were always negative and much too small. We don't think this is a units issue, however it could be. The enthalpy calculation in general seems broken considering the C_p plot shown below.

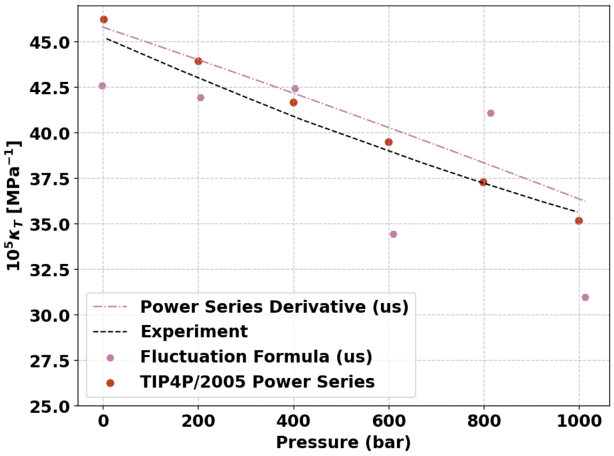

Figure 5. Isothermal compressibility κ_T at $T = 298\ K$ predicted by TIP4P/2005 as a function of temperature. The dash–dot line shows prediction to the the second order volume fit, while pink hexagon symbols give simulation values from the fluctuation formula in Eq 33. Literature data are included for comparison: TIP4P/2005 (authors: red circles polynomial), and experiment (dashed black line).

for unknown constants g, h, and i. Our results indicate

$$g = 5.10038366 \times 10^{-44}, \tag{29}$$

$$h = -4.60828990 \times 10^{-35}\ , \tag{30}$$

$$i = 1.01223245 \times 10^{-25}\ . \tag{31}$$

Note that these coefficients were fit in units of $[MPa]$ and $[m^3]$ hence their size. Taking the derivative of this gives

$$\kappa_T = 2iP + h. \tag{32}$$

Similarly to α_P there exists a fluctuation formula in the NPT ensemble given by

$$\langle \delta V^2 \rangle_{NPT} = VkT\kappa_T. \tag{33}$$

The results of this calculation are shown in Figure 5.

3.1.5 High Pressure Equation of State Due to the generalist nature of the TIP4P/2005 model the authors claim that it is sensible even at very high pressures and temperatures. We, as well as the authors, explored this behavior by computing the implied EOS. To do this we ran 7 simulations at variable temperatures (473 K and 573 K) as well as variable pressure (>1000 MPa). Again these were implemented with a LAMMPS looping procedure. We used a timestep of $dt = 1$ fs, and ran 250,000 MD steps with the first 50,000 being equilibration.

3.1.6 Phase Equilibrium Arguably, one of the most important emergent features of any interatomic potential is the multiphase behavior. Due to the vastly different local environments of solids and liquids, this can prove to be a major point of contention for most models. While TIP4P/2005 is not perfect in this regard (it generally shifts the phase diagram to lower temperatures in comparison to experiment) it still produces very accurate qualitative behavior.

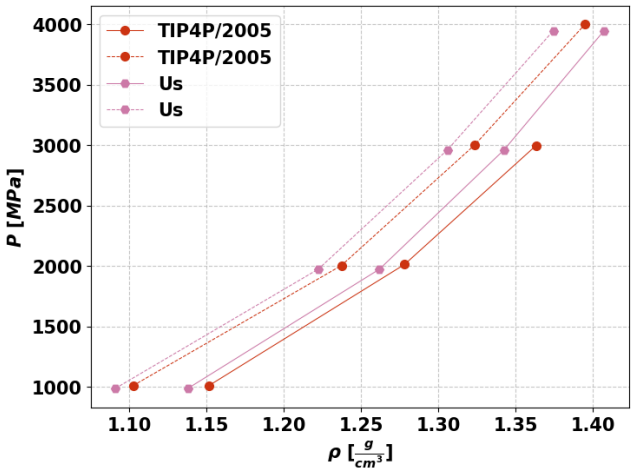

Figure 6. Pressure versus density equations of state $P(\rho, T)$ at multiple isotherms. Solid lines represent results at $T = 473\ K$, dashed lines represent results at $T = 573\ K$ (authors: red circles, us: pink hexagons).

From thermodynamics, this phase coexistence curve is traced out by the variational equation $dG = 0$ and $G_L = G_S$ in the isothermal-isobaric ensemble. This would imply we have[4]

$$dG_S = dG_L \implies -S_S dT + V_S dP = -S_L dT + V_L dP. \tag{34}$$

If we define $\Delta S = S_L - S_S$ and $\Delta V = V_L - V_S$ we have

$$\frac{\Delta S}{\Delta V} = \frac{dP}{dT}. \tag{35}$$

In an NPT ensemble we know that a change in entropy must be given by

$$dS = \frac{dQ}{T} = \frac{dH}{T} \tag{36}$$

since the change in heat is only due to a change in enthalpy at constant pressure and temperature. This result gives the Clapeyron equation as

$$\frac{\Delta H}{T\Delta V} = \frac{dP}{dT} \tag{37}$$

where the left-hand side is explicitly a function of T and P. We introduce the notation

$$\frac{\Delta H}{T\Delta V} = f(T,P) \implies \frac{dP}{dT} = f(T,P) \tag{38}$$

The enthalpy change ΔH is often referred to as the latent heat of fusion, L. These expressions suggest that, if the latent heat of fusion for the TIP4P/2005 model is known at a particular coexistence point along the implicitly defined curve $dG = 0$, the phase boundary may be extrapolated to neighboring states by integrating the differential equation given in Eq 38.

Due to the inherent numerical nature of molecular simulation we can not hope to solve this differential equation via an analytical solution. Instead we opted for a Runge-Kutta scheme. This method uses 4 evaluations of equation 38 per iteration and is defined by

$$\begin{aligned}
k_1 &= f(T_n, P_n), \\
k_2 &= f\left(T_n + \tfrac{1}{2}dT, P_n + \tfrac{1}{2}k_1 dT\right), \\
k_3 &= f\left(T_n + \tfrac{1}{2}dT, P_n + \tfrac{1}{2}k_2 dT\right), \\
k_4 &= f\left(T_n + dT, P_n + k_3 dT\right), \\
P_{n+1} &= P_n + \tfrac{1}{6}(k_1 + 2k_2 + 2k_3 + k_4)dT
\end{aligned}$$

This yields the pressure P_{n+1} for the next temperature step, $T_{n+1} = T_n + dT$. While we would have liked to use a forward difference Euler method to minimize the number of function evaluations, we found this method to quickly diverge from the curve shown in Abascal and Vega's paper. Notably, the Runge-Kutta method was also adopted by the authors for interpolation between potentials via λ.

All that remains conceptually speaking is to decipher the inference of ΔH and ΔV from a molecular simulation. To this end we attempted two different methods of calculation. The first of which was a using large box with both phases present as an initial condition. After equilibration, the resulting density distribution can then be fit to a *tanh*-like function to infer the volume of solid and liquid along the z coordinate of the box. Similarly, we can gauge the instantaneous enthalpy of each phase via a binning procedure along z. Unfortunately, this method proved to be too time consuming when combined with numerical integration. Additionally the computation of ΔH and ΔV via *tanh*-fitting was also quite unreliable in its current state due to a moving interface. In principle we expect this scheme to work, though we opted to move away from it in the interest of time.

Instead, we set up two separate simulation boxes biased by their initial condition to be in one phase or the other. By utilizing *genice2*, we were able to produce a 2000 molecule box in the *Ih* polymorph. Taking this form and melting it at high temperature produced a liquid initial condition as well. Using these boxes, we then performed two simulations with a timestep of $dt = 1$ fs with a equilibration time of 50000 fs and production of 50000 fs. From each simulation we then applied equation 20 on the instantaneous enthalpy and volume of each box to obtain the averages

$$\langle \mathcal{H} + PV \rangle_{NPT} \quad \langle V \rangle_{NPT}\,. \tag{39}$$

From the simulations we then computed $f(T,P)$ by

$$\Delta H = \langle \mathcal{H} + PV \rangle^{\mathrm{L}}_{NPT} - \langle \mathcal{H} + PV \rangle^{\mathrm{S}}_{NPT} \tag{40}$$

$$\Delta V = \langle V \rangle^{\mathrm{L}}_{NPT} - \langle V \rangle^{\mathrm{S}}_{NPT} \tag{41}$$

with S and L denoting solid and liquid quantities, respectively. This necessitates running 2 simulations per evaluation of k_i.

We opted for a $dT = -1$ to trace the L-*Ih* curve starting at T = 252.1 K, P = 1 bar. This would imply about 40 steps to arrive at the triple point between L-*Ih*-*III*. Tracing this curve would then take 320 simulations total. Ideally we would have performed this integration across all phases of ice to obtain the entire phase diagram, however we lacked the time and compute to do so. There may be a quicker and more simple method, but this was our first stride into phase diagrams via molecular simulation so we opted for a more pedagogical method.

[4] In the absence of a change in potential parameter λ.

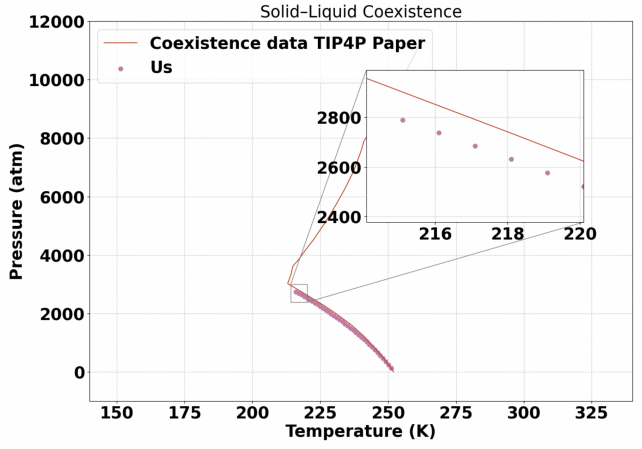

Figure 7. The solid (*Ih* ice)-liquid coexistence line traced out by equations 39. Solid line is TIP4P/2005 (authors), and pink hexagon represent our work.

3.1.7 Heat Capacity The isobaric heat capacity C_P represents the change in heat of a system as you change the temperature at constant pressure. It is given by

$$C_p = \left(\frac{\partial H}{\partial T}\right)_P. \tag{42}$$

As shown previously, the enthalpy is computed by the average instantaneous enthalpy of the box

$$H = \langle \mathcal{H} + PV \rangle_{NPT}. \tag{43}$$

The same production runs as those presented in the low-pressure isobaric density maximum are used here to calculate enthalpy as a function of T, which then allows for a power series fit of the form

$$H(T) = j + lT + mT^2 + nT^3 + pT^4 + qT^5. \tag{44}$$

This gave the coefficients as

$$j = -1.22 \times 10^5 \quad l = 1.69 \times 10^3 \quad m = -1.05 \times 10^1 \tag{45}$$

$$n = 3.31 \times 10^{-2} \quad p = -5.19 \times 10^{-5} \quad q = 3.24 \times 10^{-8} \tag{46}$$

where the polynomial was fit in units of calories per mol and kelvin. A plot of this fit is shown in figure 8, with error bars computed via the same statistical efficiency method described in 3.1.2.

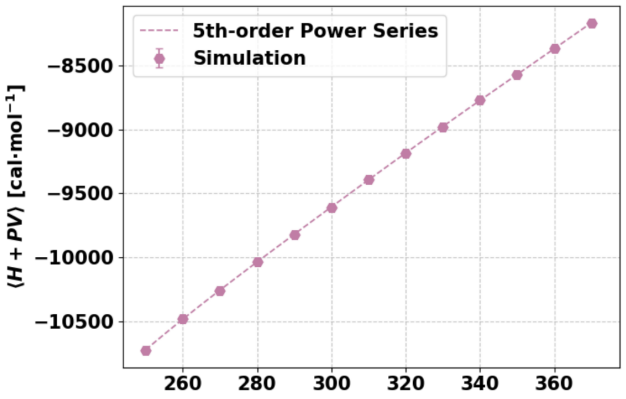

Figure 8. Mean molar enthalpy $\langle \mathcal{H} + PV \rangle$ of liquid water at $P = 1\,\text{bar}$ versus temperature. Hexagon markers show simulation averages with 95% confidence intervals (2σ error bars), and the dashed curve is a fifth–order polynomial fit later differentiated to obtain $C_p = \partial \langle \mathcal{H} + PV \rangle / \partial T$.

From this polynomial we took the temperature derivative to give the heat capacity as

$$C_p = 5qT^4 + 4pT^3 + 3nT^2 + 2mT + l. \tag{47}$$

The heat capacity also admits a fluctuation formula of the form

$$\left\langle \delta(\mathcal{H} + PV)^2 \right\rangle_{NPT} = kT^2 C_P. \tag{48}$$

The results of the derivative as well as the fluctuation formula are shown in figure 9.

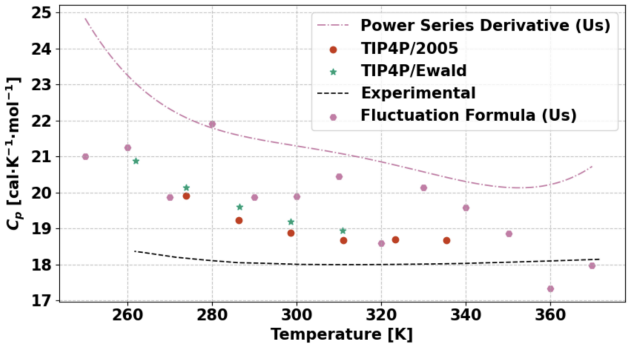

Figure 9. Isobaric heat capacity C_p of liquid water at $P = 1\,\text{bar}$ as a function of temperature. The dash–dot line shows C_p predicted by the fifth–order enthalpy fit, while pink hexagon symbols give simulation values from the fluctuation formula in Eq 48. Literature data are included for comparison: TIP4P/2005 (authors: red circles), TIP4P/Ewald (authors: green stars), and experiment (dashed black line).

3.1.8 Diffusivity Roughly speaking, the diffusivity represents how fast a fluid will disperse itself to overcome a concentration gradient. It has units of area over time and is given by

$$D = \frac{1}{3}\int_0^\infty \mathrm{d}t\ \langle \mathbf{v}_i(t) \cdot \mathbf{v}_i(0) \rangle \tag{49}$$

which over long enough time interval can be computed by

$$D = \frac{1}{6}\lim_{t\to\infty} \frac{d}{dt} \left\langle |\mathbf{r}_i(t) - \mathbf{r}_i(0)|^2 \right\rangle. \tag{50}$$

This is a particular instance of the Green-Kubo integral relations. In principle we could use any ensemble to compute D, however it is not always desirable to use the NPT ensemble we have used thus far. In order to minimize the effects on dynamics stemming from any thermo and barostats, while still computing D at the desired T and P, we use the following steps (Maginn et al., 2018).

[i] Run an NPT simulation to hit the appropriate system density and temperature.
[ii] Switch over to NVT to fix the system volume until temperature is equilibrated.
[iii] Finish with a production run in NVE and track statistics of Eq 50.

This sequence of events provides reasonable control over the thermodynamic state as well as provides a good estimate of D. We implemented the scheme outlined above in LAMMPS and then applied the *Freud* Python package for a post processing analysis of the mean squared displacement (Ramasubramani et al., 2020). We

Study	T (K)	ρ (g cm^{-3})	D (m^2 s^{-1})
This work	299.9	1.0009	3.501×10^{-9}
Exp.	291.3	n/a	1.87×10^{-9}
Exp.	291.3	n/a	1.93×10^{-9}
TIP4P/2005	297.1	n/a	2.00×10^{-9}

specifically utilized the OO pair for the computation of D. The diffusion coefficient and corresponding NVE averages are shown in the table above. A plot of the mean square displacement is shown in figure 10. The calculated value deviates quite significantly, likely due to not running enough MD steps for the timestep chosen. We only ran the final NVE simulation for around 400000 fs (0.4 ns), which may not be enough to compute an unbiased estimate for D.

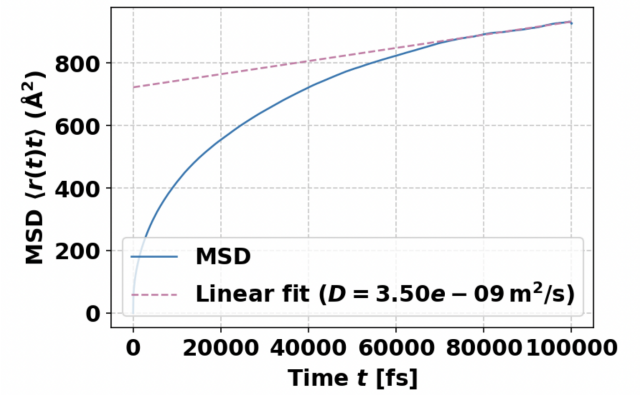

Figure 10. Mean-squared displacement of oxygen atoms versus time (fs). The dashed magenta line highlights the linear diffusive regime, yielding a diffusion coefficient D in m^2/s.

3.1.9 The Radial Distribution Function The radial distribution function (RDF) represents the local deviation in density from the ideal gas. In the NVT ensemble it can be found as an equilibrium average of the microscopic density defined by

$$\left\langle \frac{1}{N_\alpha} \sum_{i=1}^{N_\alpha} \sum_{j=1}^{N_\beta} \delta(\mathbf{r} - \mathbf{r}_j^\beta + \mathbf{r}_i^\alpha) \right\rangle_{NVT} = \rho_\beta \, g_{\alpha\beta}(r). \tag{51}$$

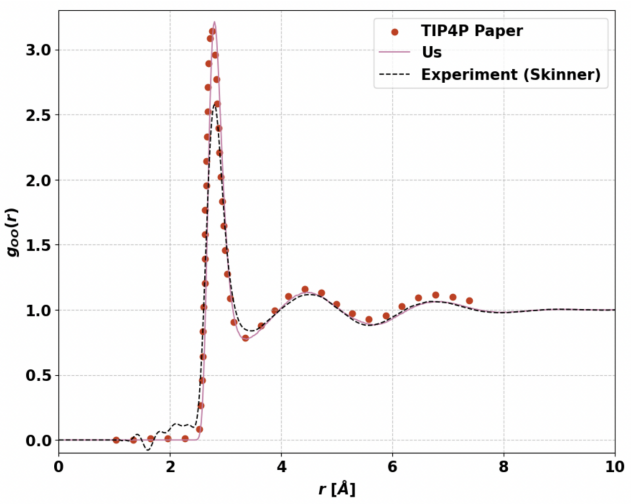

Figure 11. O-O radial distribution function $g_{OO}(r)$ for liquid water. The magenta line is from this work, red circles are TIP4P reference data, and the black dashed curve represents X–ray experiment (Skinner et al., 2013).

This function represents the probability of finding a particle of type β at a distance r from a particle of type α. In the work by Abascal and Vega they compared the OO RDF as predicted by xray and neutron scattering. We performed the same comparison via NVE simulation, specifically we utilized the same simulation as the diffusivity calculation. For post processing we again used the package *Freud* for the RDF computation. The results of this can be seen in figure 11, where a comparison is made to the experimental data.

3.2 Critical Assessment

We were successful in calculating nearly all of the target properties besides the static dielectric constant and the densities of all polymorphs. For the ones we did compute we saw significant deviation of results from those presented by Vega *et al.* Figures 3, 6, 9, and to some degree figure 5, show consistent deviation of the target properties compared to the those of authors. Even the diffusion constant D is off quite a bit. These deviations were so large that the fluctuation computation of the expansivity could not be done. A common trend was the dependence on the enthalpy. The calculations which depended on the enthalpy in a major way tended to deviate the most. This is even seen in the phase diagram reconstruction of figure 7. These differences could be due to the use of molecular dynamics instead of the Monte Carlo sampling they had performed, which tends to sample a more disordered system. There is some degree of hysteresis present in MD simulations since they have momentum, whereas MC bypasses this by sampling the appropriate distribution for the system directly.

The errors are also likely amplified by the fact that our simulations were run over a significantly smaller time scale (on the order of 1 ns, compared to their single NVE simulation of 15 million steps totaling 3.75 ns), and may not have been equilibrated enough to make accurate property estimates. The production runs we performed would no doubt benefit from at least doubling the number of MD steps, though we did initialize from a previously-equilibrated state, or nearby state, each time in an effort to combat

this. Standardizing the number of equilibration steps and production steps we used in each batch of runs would also serve as a better basis for comparison. Finally, There is also some cause for concern of our use of the Nosé-Hoover thermostat, which will necessarily change the dynamics of the system, more than, say, the Langevin method, which is stochastic. As pointed out by Tadmor, our choice of thermostat may be causing us to become stuck in regions of phase space giving a deviation from the true predictions of the potential.

Another factor was the our choice in solver for long-range interactions. We utilized the **pppm/tip4p** *k*-space style in LAMMPS, which differs from the Ewald summation technique described in the paper. This has a direct impact on the interactions of the system, and could easily cause property deviations. Overall, we have less experience than we would like with respect to modeling Coulombic interactions appropriately leading us to rely on the prebuilt LAMMPS error specification argument.

Additionally, we only investigated the liquid phase and a single polymorph of ice (*Ih*) in this work. We underestimated the amount of time (and simulations) required for generating the full phase diagram, which was a primary goal we discussed in our *proposal*. Attempting this portion earlier on, as well as constructing better shell scripts to automate a majority of it would have helped greatly with the ability to compute different portions of the diagram in parallel.

4 Conclusions

4.1 Summary

In this article, we present our efforts in recreating the seminal work by Abascal et al., 2005, using their rigid, 4-site TIP4P/2005 model of water to calculate a wide variety of thermodynamic properties with near-experimental accuracy. Namely, we were able to reproduce liquid density as functions of T and P ($\rho(T)$, $\rho(P)$), thermal expansivity (α_P), isothermal compressibility (κ_T), liquid-phase pair distribution function ($g_{OO}(r)$), the liquid self-diffusion coefficient (D), the L-*Ih* polymorph phase equilibrium line, constant pressure heat capacity C_p, and a high pressure equation of state ($P(\rho)$), with decent success. The bulk of the simulations were performed in an NPT ensemble (the calculation of self-diffusion requiring NVE) utilizing GPUs from the MSI's Agate cluster where possible. All runs used some semblance of Python or SLURM scripting to enable high-throughput computing and automated sweeps over input conditions.

4.2 Future Work

Provided more time and resources, there are a few things that we would like to investigate further. Firstly, Vega and Abascal compare and contrast the results of many other popular water models, namely SPC, SPC/E, TIP3P and other TIP4P variants. These all differ in particular geometry, accuracy and predictive capabilities, with some apparently not being able to reproduce certain phenomena such as a temperature of maximum density T_{md}. Being able to implement all of these models successfully in MD simulations, as well as to recreate results across multiple articles, would have served as a great learning exercise.

We also would have preferred to spend more time resolving the differences observed between our MD and their MC results. Similarly a study of the different polymorphs could have revealed where our simulations were lacking as the only solid phase we considered was the hexagonal structure. Another possible avenue for future work is a reproduction of the optimization procedure with more rigorous uncertainty quantification and possibly a more globally optimal method such as Markov Chain Monte Carlo optimization. This can help decipher questions such as, is this the only TIP4P like model that can reproduce these QOIs, as well as ensure the parameters are well conditioned by the experimental data.

5 Special Thanks

Thanks to Ellad Tadmor for the helpful advice and slides regarding molecular simulation. Thanks also to David Morse and Porhouy Minh for the discussions and advice on phase diagram reconstruction, as well as Axel for providing their expertise with LAMMPS in many forum posts.

References

Abascal, J. L. F. and C. Vega (Dec. 2005). "A general purpose model for the condensed phases of water: TIP4P/2005". In: *The Journal of Chemical Physics* 123.23, p. 234505. ISSN: 0021-9606. DOI: 10.1063/1.2121687. eprint: https://pubs.aip.org/aip/jcp/article-pdf/doi/10.1063/1.2121687/15377081/234505_1_online.pdf. URL: https://doi.org/10.1063/1.2121687.

Allen, Michael P. and Dominic J. Tildesley (June 2017). *Computer Simulation of Liquids*. Oxford University Press. ISBN: 9780198803195. DOI: 10.1093/oso/9780198803195.001.0001. URL: https://doi.org/10.1093/oso/9780198803195.001.0001.

Frenkel, Daan and Berend Smit (2002). "Chapter 7 - Free Energy Calculations". In: *Understanding Molecular Simulation (Second Edition)*. Ed. by Daan Frenkel and Berend Smit. Second Edition. San Diego: Academic Press, pp. 167–200. ISBN: 978-0-12-267351-1. DOI: https://doi.org/10.1016/B978-012267351-1/50009-2. URL: https://www.sciencedirect.com/science/article/pii/B9780122673511500092.

Gibbs, Mark N (1998). "Bayesian Gaussian processes for regression and classification". PhD thesis. Citeseer.

Jacobson, Liam C., Robert M. Kirby, and Valeria Molinero (2014). "How Short Is Too Short for the Interactions of a Water Potential? Exploring the Parameter Space of a Coarse-Grained Water Model Using Uncertainty Quantification". In: *The Journal of Physical Chemistry B* 118.28. PMID: 24605768, pp. 8190–8202. DOI: 10.1021/jp5012928. eprint: https://doi.org/10.1021/jp5012928. URL: https://doi.org/10.1021/jp5012928.

Maginn, Edward J. et al. (Dec. 2018). "Best Practices for Computing Transport Properties 1. Self-Diffusivity and Viscosity from Equilibrium Molecular Dynamics [Article v1.0]". In: *Living Journal of Computational Molecular Science* 1.1, p. 6324. DOI: 10.33011/livecoms.1.1.6324. URL: https://livecomsjournal.org/index.php/livecoms/article/view/v1i1e6324.

Matsumoto, Masakazu, Takuma Yagasaki, and Hideki Tanaka (2024). "GenIce-core: Efficient algorithm for generation of hydrogen-disordered ice structures". In: *Journal of Chemical Physics* 160, p. 094101.

Paschek, Dietmar (Apr. 2004). "Temperature dependence of the hydrophobic hydration and interaction of simple solutes: An examination of five popular water models". In: *The Journal of Chemical Physics* 120.14, pp. 6674–6690. ISSN: 0021-9606. DOI: 10.1063/1.1652015. eprint: https://pubs.aip.org/aip/jcp/article-pdf/120/14/6674/19122346/6674_1_online.pdf. URL: https://doi.org/10.1063/1.1652015.

Ramasubramani, Vyas et al. (2020). "freud: A Software Suite for High Throughput Analysis of Particle Simulation Data". In: *Computer Physics Communications* 254, p. 107275. ISSN: 0010-4655. DOI: https://doi.org/10.1016/j.cpc.2020.107275. URL: http://www.sciencedirect.com/science/article/pii/S0010465520300916.

Rasmussen, Carl Edward and Christopher K. I. Williams (2008). *Gaussian processes for machine learning Carl Edward Rasmussen; Christopher K.I. Williams*. MIT Press.

Skinner, Lawrie B. et al. (Feb. 2013). "Benchmark oxygen-oxygen pair-distribution function of ambient water from x-ray diffraction measurements with a wide Q-range". In: *The Journal of Chemical Physics* 138.7, p. 074506. ISSN: 0021-9606. DOI: 10.1063/1.4790861. eprint: https://pubs.aip.org/aip/jcp/article-pdf/doi/10.1063/1.4790861/14046674/074506_1_online.pdf. URL: https://doi.org/10.1063/1.4790861.

Vega, C. and J. L. F. Abascal (Oct. 2005). "Relation between the melting temperature and the temperature of maximum density for the most common models of water". In: *The Journal of Chemical Physics* 123.14, p. 144504. ISSN: 0021-9606. DOI: 10.1063/1.2056539. eprint: https://pubs.aip.org/aip/jcp/article-pdf/doi/10.1063/1.2056539/15376017/144504_1_online.pdf. URL: https://doi.org/10.1063/1.2056539.